Characterization of neutralized graphite oxide and its use in electric double layer capacitors

CrossMark

Wenwen Zhao, Gentoku Kido, Kazuki Hara, Hideyuki Noguchi *

Department of Applied Chemistry, Saga University, Honjo-1, Saga 840-8520, Japan

ABSTRACT

Spherical graphite oxide (GO) with high density was synthesized from mesocarbon microbeads (MCMB). The obtained GO was neutralized by various alkaline metal hydroxides and tetraalkylammonium hydroxides. The neutralized GO showed lower water content and much better thermal stability than those of pristine GO. The as-prepared neutralized GOs were investigated as electrode materials for electric double layer capacitor (EDLC) in organic electrolyte. From both the results of galvanostatic charge–discharge and cyclic voltammetry (CV) measurements, it was found that the tetrabutylammonium hydroxide (TBA-OH) together with lithium hydroxide neutralized GO (TBA-Li-GO) displayed a relatively ideal EDLC feature after electrochemical activation at the initial cycle. The positively polarized TBA-Li-GO with small surface area ($16 \, \mathrm{m^2 \, g^{-1}}$) exhibited a high volumetric capacitance of $60 \, \mathrm{F \, cm^{-3}}$ after 1000 cycles, which is much higher than that of commercial activated carbon ($36 \, \mathrm{F \, cm^{-3}}$).

1. Introduction

Electric double layer capacitors (EDLCs) have attracted a considerable attention during the past several decades owing to their extremely high power density and long cycle life. Due to the intrinsic nature of EDLC, it has been considered as a good candidate for high power devices, especially for automotive applications [1–4]. Carbon based materials such as activated carbons [5–7], activated carbon fibers [8,9], carbon aerogels [10,11] and carbon nanotube [12,13] have been studied intensively for the use as electrode materials for EDLCs. Among these carbonaceous materials, porous activated carbons with high surface area ($1000–2000 \, \mathrm{m^2 \, g^{-1}}$) are considered to be the most ideal electrode material for EDLC. It has been proved that the activated carbons show good cycleability and stability in a great variety of electrolytes. However, due to the large surface area and high porosity of activated carbons, the volumetric capacitance of the commercial activated carbon is still in a low level [14,15].

In the past several years, graphene based material has attracted great attention from many researchers because of its exceptional properties and potential applications in energy storage devices [16,17]. Graphene oxide, which is generated from graphite oxide

(GO), has been a promising approach to prepare graphene related materials. Furthermore, the reduced graphene oxide has been studied intensively by many researchers for the use as an electrode material for electrochemical capacitors [18,19]. Although high gravimetric energy density can be obtained in these devices, the volumetric energy density of grapheme based electrode materials is still low because of their porous texture does not allow the dense packing. Only a few works have successfully obtained electrode materials with both high gravimetric and high volumetric capacitance in reduced grapheme oxide [20,21]. Therefore, it is of great necessity to develop high density electrode materials for EDLC.

Herein, we focused on the synthesis of graphite oxide with lamellar structure by selecting mesocarbon microbeads (MCMB) as starting material. MCMB has been recognized as an excellent precursor for the synthesis of high density and high strength carbonaceous material since it was first separated from mesophase pitches by Yamada et al. [22]. The spherical shape of MCMB particles with lamellar graphene sheet would be ideal for approaching dense packing. Zheng et al. have investigated non-porous activated MCMB as the negative electrode for asymmetric electrochemical capacitors with improve energy and power density [23]. Moreover, high content of sp^3 carbon in MCMB may inhibit the exfoliation of graphene layers during the chemical oxidation so as to retain the high density. It is also well known that various oxygen functional groups are introduced into layers of graphene sheets after oxidation. Due to the existence of some acidic groups, such as COOH and phenolic OH, GO can be neutralized by various alkaline hydroxides as well as tetraalkylammonium hydroxides. In this study, various neutralized GOs with high tap density were

* Corresponding author. Tel.: +81 952 28 8674; fax: +81 952 28 8591.
E-mail address: noguchih@cc.saga-u.ac.jp (H. Noguchi).

successfully prepared. Despite of the extremely low surface area, non-porous neutralized GO showed much higher volumetric capacitance than that of activated carbon. Furthermore, compared to the synthetic methods of activated carbons, our method is easy to operate, very fast, low cost and without the need of chemical activation at high temperature.

2. Experimental

2.1. Preparation of graphite oxide

GO was synthesized from MCMB (average particle size: 15 μm, Hosen Co., Japan) according to the traditional Hummers method [24]. Typically, MCMB (10 g) and $NaNO_3$ (5 g) together with H_2SO_4 (220 mL) were mixed in a round flask placed into the water ice bath. To avoid vigorous reaction, $KMnO_4$ (20 g) was gradually added into the mixture at 0–10 °C. After the addition of $KMnO_4$, the mixture was kept at 35 °C for 1 h. Subsequently, the mixture was transferred to 460 mL H_2O and hold strictly at 98 °C for 30 min. The reaction was terminated by adding 1400 mL H_2O and 10 mL H_2O_2. Then the diluted solution was kept for 1 day followed by filtering and drying at 80 °C for 12 h.

2.2. Preparation of neutralized GO

For the preparation of neutralized GO, the obtained GO (1.0 g) was dispersed in 100 mL H_2O. The dispersion was stirred and then titrated with various alkaline hydroxides solution (0.2 M) and tetraalkylammonium hydroxides solution (0.24 M) until the pH = 11. The whole process was controlled considerably slow to enable the fully neutralization of GO. The reaction was kept at 25 °C for another 3 h. Then, neutralized GO powder can be obtained after filtering and drying at 80 °C for 12 h.

2.3. Characterization methods

X-ray diffraction (XRD) profiles of the as-prepared GO and neutralized GOs were recorded for two theta value from 3° to 80° (Cu Kα radiation, XRD-7000, SHIMADZU). Thermo-Gravimetric/Differential Thermal Analysis (TG-DTA) measurement was performed at a heating rate of 5 °C min^{-1} from room temperature to 500 °C in air (Thermoflex TG-DTA 8110, Rigaku). Fourier transform infrared spectroscopy (FTIR) spectra of the samples were recorded on a JASCO 400 FTIR spectrometer (KBr pellets method). Nitrogen adsorption–desorption isotherm were carried out after the samples were outgassed and dehydrated at 180 °C for 24 h (Micromeritics Gemini 2360, SHIMADZU). The specific surface area of each sample was calculated from the Brunauer–Emment–Teller (BET) method. Mercury intrusion porosimetry measurements were performed on a Micromeritics AutoPore III 9420 mercury porosimeter (SHIMADZU). The tap density is achieved by mechanically tapping a measuring cylinder containing a power sample. After observing the initial volume, the cylinder is mechanically tapped, and volume readings are taken until little further volume change is observed. Generally, replicate measurements were carried out for the determination of tap density.

2.4. Electrochemical characterization of GO and neutralized GO

The symmetric capacitors of neutralized GO and commercial activated carbon (AC1, Kuraray Chemical Co., Japan) were examined by using the CR-2032 type coin cell with 1 M triethyl-methyl-lammonium phosphorus hexafluoride (TEMAPF$_6$) as electrolyte. For the fabrication of electrodes, 10 mg active material together with 4 mg conducting binder (Teflon:Acetylene black = 1:2) was

mixed and pressed on the stainless steel mesh. Then, the electrodes were dehydrated by a vacuum dry at 150 °C for 12 h. The cell was cycled between 0 and 3 V at a current density of 0.8 mA cm^{-2}. The specific capacitance of the symmetric capacitors was estimated according to the following equations [25]:

$$C_m = (I \times \Delta t)/(\Delta V \times m) \tag{1}$$

$$C_{sp} = 4C_m \tag{2}$$

where C_m is the measured capacitance of the electrode (F g^{-1}), Δt is the discharge time (s), ΔV is the potential window during the discharge process (V), m is the total weight of the active material on the two electrodes, C_{sp} refers to the specific capacitance of a single electrode in two electrodes cell.

The cyclic voltammetry (CV) measurements were conducted under three electrode cells with lithium metal as both reference and counter electrode. The electrolyte used was a mixture of 1 M lithium phosphorus hexafluoride (LiPF$_6$) and 1 M TEMAPF$_6$ in propylene carbonate with volume ration of 1:5. The capacitance estimated from CV (C_{cv}) was calculated according to following equation:

$$C_{cv} = \left(\int idV \right) / v\Delta Vm \tag{3}$$

where i is the response current (A), v is the scan rate (V s^{-1}), ΔV is the potential window (V) and m is the weight of the electrode material (g).

To investigate the electrochemical activation of TBA-Li-GO electrode, galvanostatic charge–discharge measurement was examined in a half cell with lithium metal as counter and reference electrode. In this case, the electrolyte used was a mixture of 1 M lithium phosphorus hexafluoride (LiPF$_6$) and 1 M TEMAPF$_6$ in propylene carbonate (PC) with volume ration of 1:5. The electrodes were fabricated with the same method as that used in symmetric capacitors. Electrochemical impedance spectroscopy (EIS) was recorded with the potential amplitude of alternative current was 10 mV and the frequency range was from 50 kHz to 10 mHz.

3. Results and discussion

3.1. Characterization of GO

The XRD patterns of pristine MCMB and GOs are shown in Fig. 1. Pristine MCMB shows a very sharp diffraction peak at $2\theta = 26°$
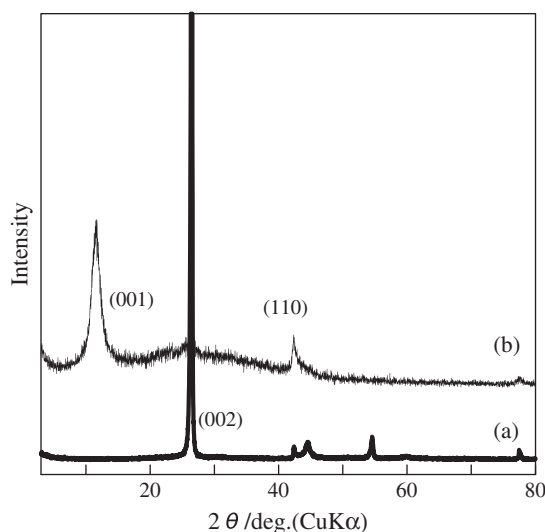

Fig. 1. XRD patterns of pristine MCMB and GO: (a) pristine MCMB, (b) GO.

Table 1
Elemental analysis and physical properties of MCMB and GO.

Sample	Elemental analysis				Surface area	Pore volume
	H	C	N	O	S_{BET} (m^2 g^{-1})	V (cm^{-3} g^{-1})
MCMB	0.02	99.92	–	0.06	3	0.02
GO	1.09	62.59	0.11	36.21	14	0.12

which is the characteristic peak of graphite. This peak corresponds to the diffraction of the (002) plane, being the interlayer distance, d_{002} = 0.337 nm. After oxidation, pristine graphite loses its original intensive peak 2θ = 26° and new peak at around 2θ = 12° appears, which indicates that the oxidation of graphite causing a transformation of the crystalline structure into a new one with a wider d-spacing. Such a large shift towards lower angle has been proved to be due to the introduction of water into interlayers of graphite oxide [26]. The interlayer spacing of GO prepared by us is found to be around 0.78 nm, which is in accordance with the results presented by many literatures [27,28]. Table 1 gives the elemental analysis results, BET surface area and pore volume of pristine MCMB and GO. The content of oxygen increases greatly in GO, which also suggests the oxidation of MCMB. Moreover, both the surface area and pore volume increases after oxidation.

In order to investigate the morphology change after mild oxidation, the SEM measurement was carried out. Fig. 2 shows the SEM images of pristine MCMB and GO. The average particle size of MCMB is around 15 μm and very rough surface can be observed. As it was expected, GO keeps the spherical shapes even after mild oxidation. From the larger magnification SEM images it is obviously to see that some cracks with pore diameter around 5–10 μm are generated on the surface of GO. These cracks generated through oxidation may cause the increase of the surface area as shown in Table 1.

Since some cracks can been generated in GO through oxidation, we tried to determine the average pore size of these cracks by using mercury intrusion porosimetry, which can give a precise evaluation of the diameter of the cracks. Fig. 3 presents the results of mercury intrusion porosimetry obtained from pristine MCMB and GO. The pore diameter of pristine MCMB is around 2–3 μm, which might be due to the free space generated between the spherical particles. On the other hand, the diameter of cracks generated in GO is found to be around 5–8 μm. This value is in good agreement with the value estimated from the SEM images.

3.2. Characterization of neutralized GOs

It is well known that GO contains various functional groups, such as COOH, OH, C=O and C—O—C. Therefore, the acidic groups in GO can be neutralized by various bases. Acid–base titration is a powerful tool to determine the content of acidic groups in GO, such as COOH and phenolic OH groups [29,30]. The pH titration curves of GO with alkaline hydroxides and tetraalkyl-ammonium hydroxides (tetrametylammonium hydroxide, TMAOH, or tetrabutylammonium hydroxide, TBAOH) are shown in Fig. 4. Alkaline metal hydroxides, LiOH, NaOH and KOH, give similar titration curves, in which continuous increase in pH value is observed against the amount of the added bases. The ion exchange capacity of GO estimated at pH = 11 is roughly 3 mmol g^{-1}, which is smaller than the value reported by Matsuo et al. [31] (3.5 mmol g^{-1}) and Liu et al. [32] (4.4 mmol g^{-1}). Szabo et al. [33] has investigated the ion exchange capacity of GO and pointed out that the value varies in a wide range, depending not only on the synthesis method, but also the pH and ionic strength. The ion exchange capacities by ammonium hydroxide give smaller values, which are 2.0 and 1.3 mmol g^{-1} for TMAOH ((CH_3)$_4$NOH) and TBAOH ((C_4H_9)$_4$NOH), respectively. In other words, larger tetrabutylammonium ion (TBA$^+$) gives smaller capacity. Those results would be easily
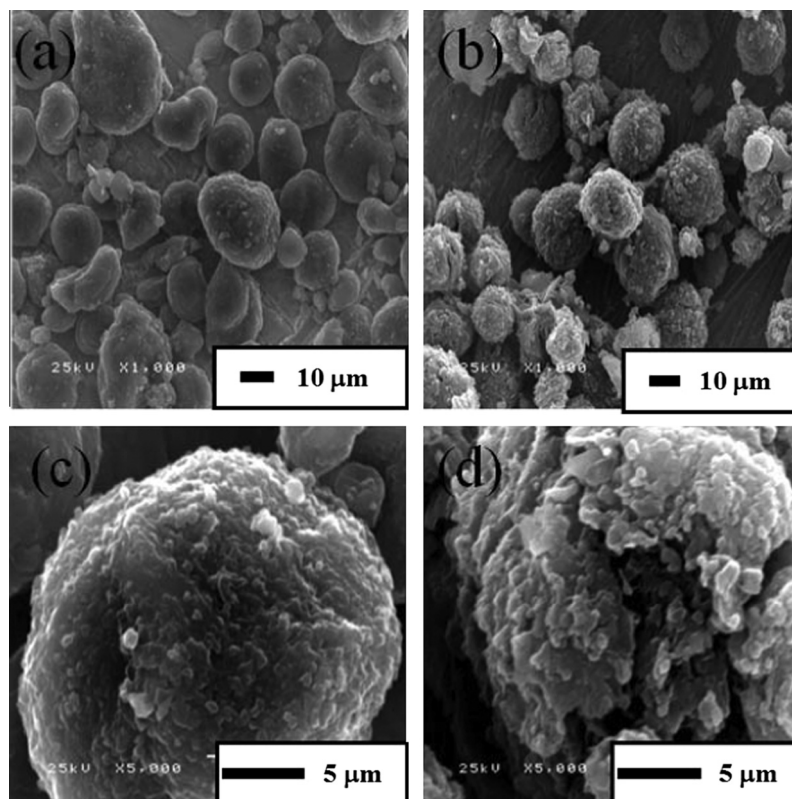

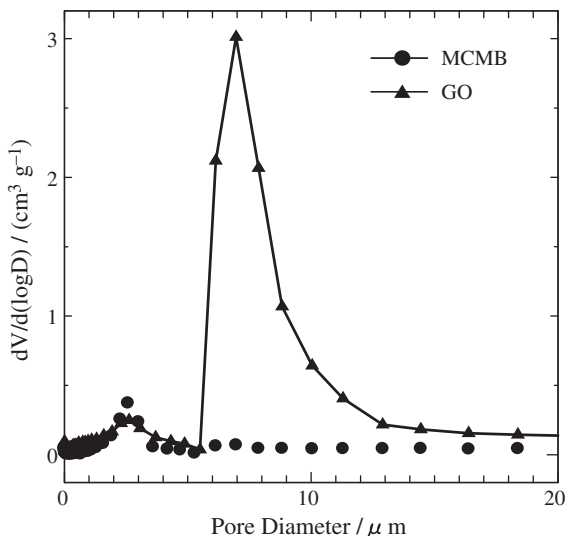**Fig. 2.** SEM images of pristine MCMB and GO: (a and c) pristine MCMB, (b and d) GO.

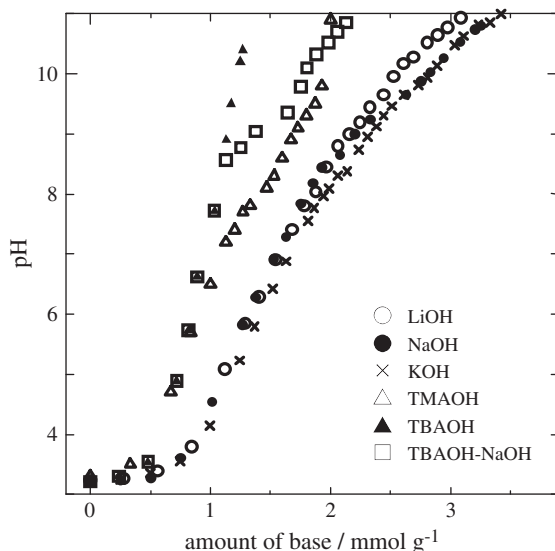**Fig. 3.** Mercury intrusion porosimetry results of MCMB and GO.

Fig. 4. The pH titration curves of GO by various bases.

molecules and to the hydroxyl groups of GO [34]. A band at 1760 cm^{-1} was assigned to be the C=O stretching vibrations of the —COOH groups and the following band at 1600 cm^{-1} would be considered to be the vibration of C=C [35]. A weak peak located at 1350 cm^{-1} was assigned to be the OH bending of the C—OH groups [34]. A strong band at 1100 cm^{-1} might be attributed to C—O stretching vibration [35–37]. However, in the case of LiOH neutralized GO (Li-GO), the prominent COOH peak at 1760 cm^{-1} almost disappeared and only C=O stretching band was detected. The decrease of acidic functional groups indicates neutralized GO was obtained. The intensity of the broad band at approximately 3500 cm^{-1} assigned to OH was also weakened. In the TBAOH neutralized GO (TBA-GO), the prominent bands at 2900 and 2850 cm^{-1} due to the symmetric and asymmetric vibration of the C—H groups and the peak located at 1360 cm^{-1} corresponding to C—N vibration can be observed, which support the existence of TBA ions [38]. Meanwhile, in the TBAOH–LiOH neutralized GO (TBA-Li-GO), the
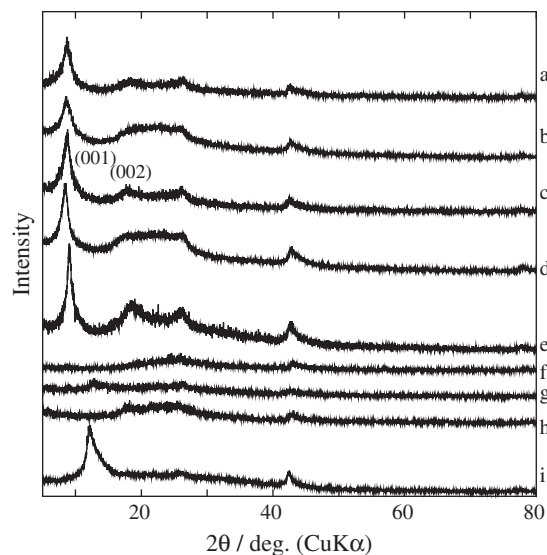

Fig. 5. XRD patterns of GO and neutralized GOs:(a) TBAOH–KOH, (b) TBAOH–NaOH, (c) TBAOH–LiOH, (d) TBAOH, (e) TMAOH, (f) KOH, (g) NaOH, (h) LiOH, (i) GO.
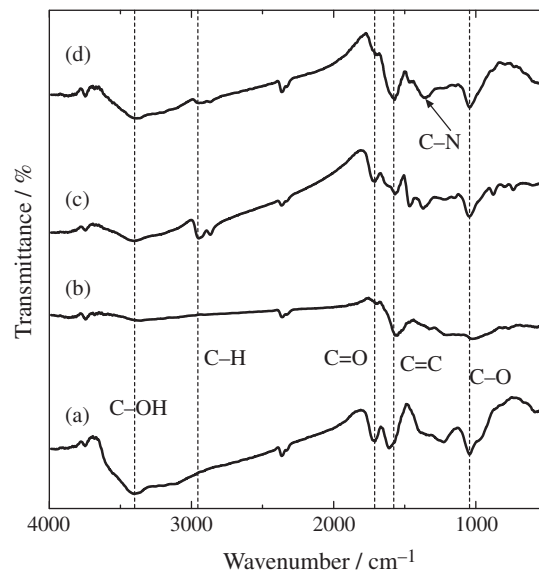
explained by considering the intercalation of ammonium ion into GO layers. Also, it is worth noting that the combinations of TBAOH with LiOH and KOH give similar pH titration curves.

Fig. 5 presents the XRD patterns of GO and neutralized GOs by various bases. The profiles of neutralized GOs with alkaline metal hydroxide and tetraalkylammonium hydroxide are completely different. When GO is treated with alkaline metal hydroxide, the characteristic peak at around 2θ = 12° disappeared, which would be due to removal of intercalated water in GO. On the other hand, TBAOH neutralized GO (TBA-GO) exhibits new peak at 2θ = 10°. The d spacing of the lowest peak is found to be 1.0–1.02 nm, which is 20% larger than that of pristine GO. The appearance of the new peak would support the intercalation of TBA ions between the layers of GO. Meanwhile, TBA-Li-GO, TBA-Na-GO and TBA-K-GO give the similar XRD profiles as that of TBA-GO, which also support the intercalation of TBA ions in GO.

Fig. 6 shows the FT-IR spectra of GO and neutralized GOs. The presence of various oxygen functional groups in GO is confirmed by FT-IR spectra. A broad band at 3000–3700 cm^{-1} was contributed to the presence of hydroxyl groups, due to the water

Fig. 6. FT-IR spectra of (a) GO, (b) Li-GO, (c) TBA-GO, and (d) TBA-Li-GO.
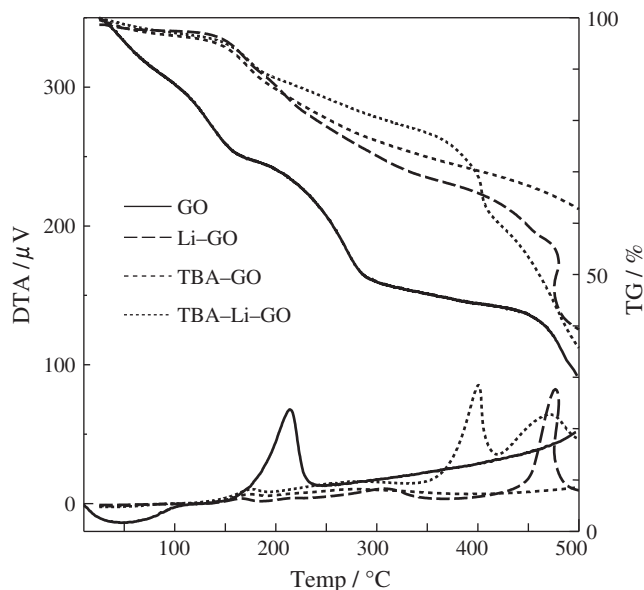
Fig. 7. TG/DTA analysis of GO and neutralized GOs.

decrease of the peak at 1760 cm^{-1} and the observation of TBA ions are also obvious.

We have found that when GO is heated at around 200 °C, it decomposed explosively and changed to fine particles. Such an explosive reaction of massive GO causes the increase in both pore volume and surface area has been reported [39]. Stability of GO against heat-treatment at around 180 °C under the vacuum allows it to use safely as electrode material for capacitor using organic electrolyte. Therefore, it is of great importance and necessity to further investigate the thermal property of GO and neutralized GOs.

Fig. 7 gives TG/DTA profiles of GO and neutralized GOs. Release of water would occur at less than 175 °C, which is accompanied with a broad endothermic peak in DTA profile. The total mass loss of GO below 175 °C was around 30%. Sharp weight loss together with an exothermic peak in DTA profile around 200 °C, suggesting the violent decomposition of some oxygen functional groups in GO. Further, weight loss at more than 400 °C is attributed to the burning of GO in air.

On the other hand, weight loss of neutralized GOs below 175 °C decreased to about 5%. Furthermore, in the neutralized GOs, the strong exothermic peaks observed in DTA profile of GO vanished. Above different thermal characters between GO and neutralized GOs suggest that the thermal stability of GO is improved significantly after neutralization. The improved thermal stability of neutralized GOs can enable the further heat treatment safely.

3.3. Electrochemical characterization of GO and neutralized GOs

Since TBA-Li-GO shows larger interlayer distance and low water content, we tried to use it as electrode materials for electric double layer capacitor (EDLC). The EDLC features of TBA-Li-GO are presented in Fig. 8(d). For comparison, commercial activated carbon (AC1), GO and lithium hydroxide neutralized GO (Li-GO) were also tested. The charge and discharge curves of AC show good linearity in all cycles, which is a typical feature of EDLC. For pristine GO, bend curve can be observed at around 1.3 V. The observed capacitance would be due to the electrochemical decomposition of water or oxygen functional groups remained in GO. The rapid decrease in capacitance in the following cycles also suggests that the faradic reaction might occurred in pristine GO. In the case of Li-GO, ideal EDLC feature was obtained though the capacitance is rather small than that of AC1. The capacitance remained almost the same in the subsequent cycles. The improved electrochemical properties for Li-GO would be attributed to the lower water content and stabilization of oxygen functional groups after neutralization. In
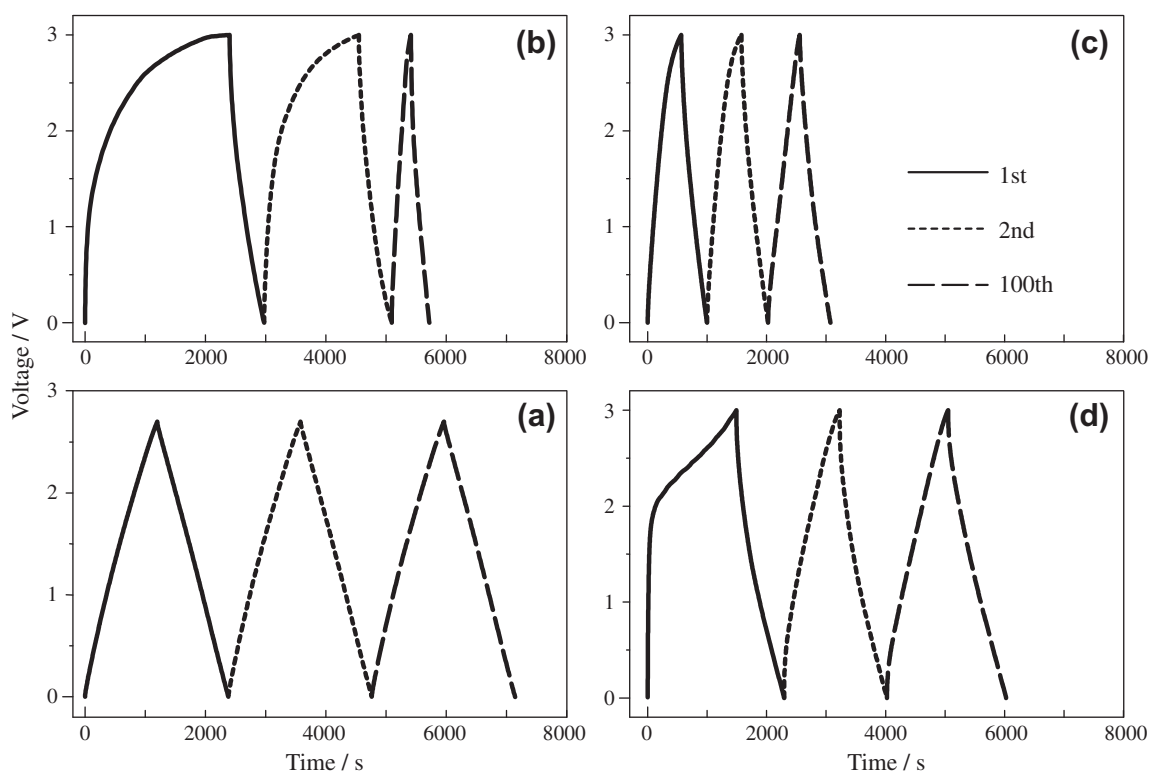

Fig. 8. Galvanostatic charge and discharge curve of (a) AC1, (b) GO, (c) Li-GO and (d) TBA-Li-GO symmetric capacitors.
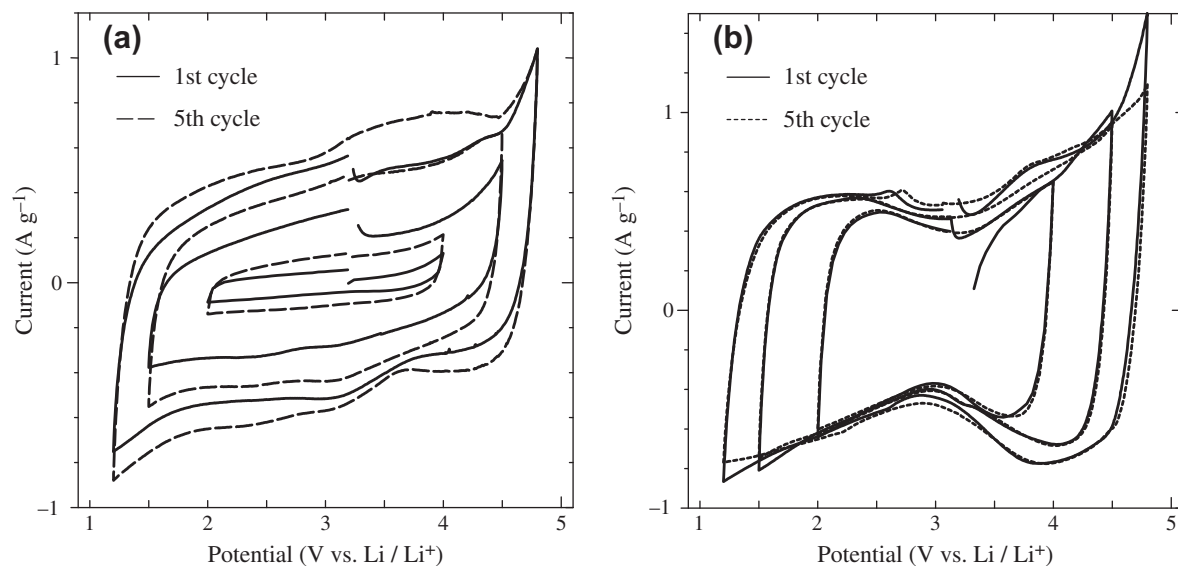
Fig. 9. Cyclic voltammogram of TBA-Li-GO (a) and AC1 (b) under various potential ranges at scan rate of 5 mV s^{-1}.
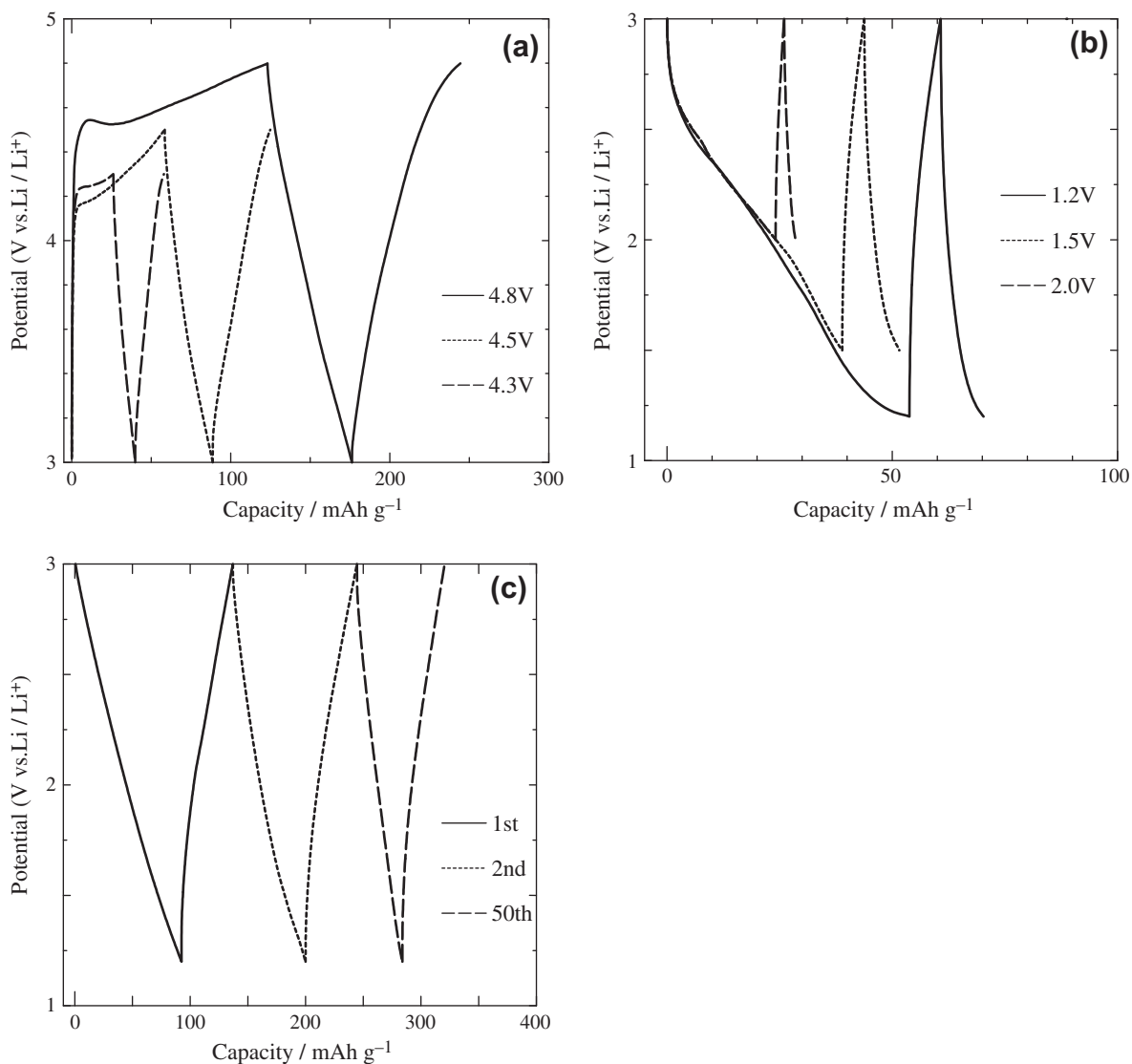

Fig. 10. Galvanostatic charge and discharge voltage profiles of TBA-Li-GO cycling from (a) OCV to 4.3 V, 4.5 V, 4.8 V; (b) OCV to 2.0 V, 1.5 V, 1.2 V; (c) positively polarized TBA-Li-GO electrode cycling between 3 V and 1.2 V.
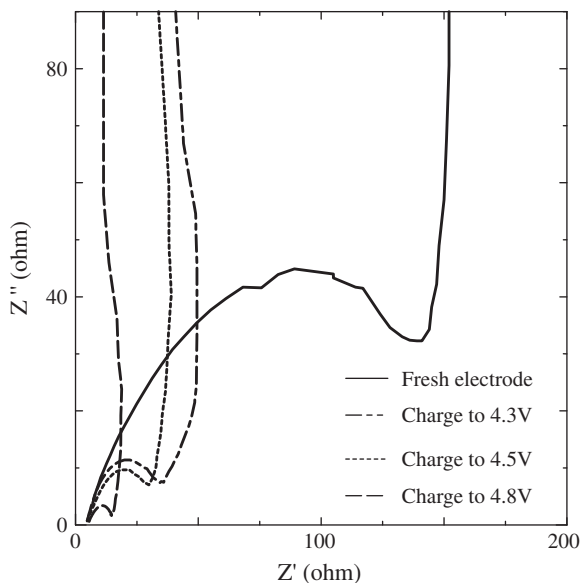
Fig. 11. Impedance spectra of TBA-Li-GO electrode cycled between OCV and 4.3 V, 4.5 V, 4.8 V.

contrast, TBA-Li-GO exhibits a different charge profiles at the first charge process. It is worth noting that very small capacity of TBA-Li-GO is observed below 2 V, suggesting that negligible small double layer was formed when the non-porous carbon was dipped into the electrolyte solution. However, a voltage plateau appears in the voltage range between 2 and 3 V. Due to the appearance of this voltage plateau, the capacitance below 2 V increases greatly in the following cycles. Similar results have been reported by Kim et al. [39] and Takeuchi et al. [40,41] previously. The increasing capacitance is said to be associated with the intercalation of electrolyte ions between the internal layers after electrochemical activation at the first charge. It is seems that the neutralized GO in our work can also be activated electrochemically.

In order to further investigate the electrochemical properties of TBA-Li-GO, cyclic voltammetry (CV) measurement was carried out. Fig. 9(a) and (b) present the CV curves of TBA-Li-GO and activated carbon (AC1) in various voltage ranges at the scan rate of 5 mV s^{-1}. When the potential range was set between 2.0 and 4.0 V, only a small value of current was observed. Also, it is obvious that the current value increased after 5 cycles. Furthermore, when we enlarge the potential range to 1.5–4.5 V and 1.2–4.8 V, it is interesting to find that the current increased gradually with the increasing of working voltage. Meanwhile, it is clear to see that the current increased upon cycling. However, from the CV curves of AC1 we can find that there is no obvious increasing of current upon cycling. The above results reveal that electrochemical activation process occurred for the TBA-Li-GO sample when it was cycling at wider working voltage range. This phenomenon has been reported by Hantel et al. [21], in which they demonstrated that the partially reduced graphite oxide exhibited a increasing of capacitance while treated at specific activation potential.

However, we cannot give a possible explanation for this activation process only from the CV measurement. In order to elucidate the mechanism for the increased capacitance, galvanostatic charge–discharge tests of a single TBA-Li-GO electrode were performed. The potential range were set from the open circuit potential (OCV) to 4.3 V, 4.5 V, 4.8 V as well as to 2.0 V, 1.5 V, 1.2 V. Fig. 10(a) and (b) display the charge and discharge curves of TBA-Li-GO electrode cycled as positive and negative electrode, respectively. As shown in Fig. 10(a), the appearance of voltage

plateau at the initial charge are observed in all the three potential ranges. As it was mentioned above, such voltage plateau also appeared at the first charge profile of symmetric capacitors. If the electrode was first positively polarized at high potential, non-faradic capacity increased significantly in the subsequent cycles. The increased capacitance for TBA-Li-GO at a wider potential range is in good agreement with the results of CV measurement. Since it was revealed that electrochemical activation of TBA-Li-GO by positive polarization at high potential is very effective activation process, we tried to further study the effect of negative polarization. As it is shown in Fig. 10(b), different from positive polarization, this is no appearance of voltage plateau even though the electrode was discharge to 1.2 V. Furthermore, although the capacity of TBA-Li-GO slightly increased at larger potential range, the capacity is much lower than that after positive polarization.

Another independent experiment was carried out to investigate the effect of positive polarization. At first, a new TBA-Li-GO electrode was positively polarized at 4.8 V and then discharge to 3 V in a half cell. After a certain rest time, the positively polarized electrode was then cycled between 3 V and 1.2 V. The obtained charge and discharge profiles of the polarized electrode are shown in Fig. 10(c). As it was described in Fig. 10(b), the TBA-Li-GO electrode delivered very small capacity when it was cycled between 3 V to 1.2 V. However, as shown in Fig. 10(c), the discharge capacity of the polarized TBA-Li-GO electrode increased to about 100 mA h g^{-1}. Moreover, it delivered a much higher capacity in the subsequently cycles than that of the electrode without positive polarization. Therefore, based on the above results, we believe that the increased capacitance of TBA-Li-GO electrode at wider potential range should be mainly attributed to the electrochemical activation by positive polarization. The neutralized GO in this study seemed to be more sensitive to positive polarization than negative polarization, which is a little different from that of oxidized meso-carbon microbeads by Oh et al. [42]. As it was pointed out by Hantel et al. [43], beside the influence of interlayer distance of carbon materials, the chemical composition of electrode material and the electrolyte solution seems to affect the electrochemical activation and thus the capacitance.

It is possible that the positive polarization of TBA-Li-GO electrode would also generate new sites which are accessible for the electrolyte ions. Due to the generation of the new sites, it could be expected that the ion transfer resistance of polarized electrode would decrease, which would facilitate the adsorption of
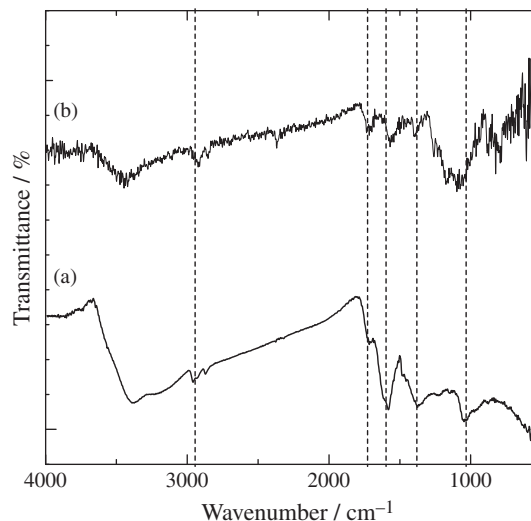

Fig. 12. Ex situ FTIR profiles of pristine TBA-Li-GO electrode (a) and TBA-Li-GO electrode after cycling between OCV and 4.8 V (b).
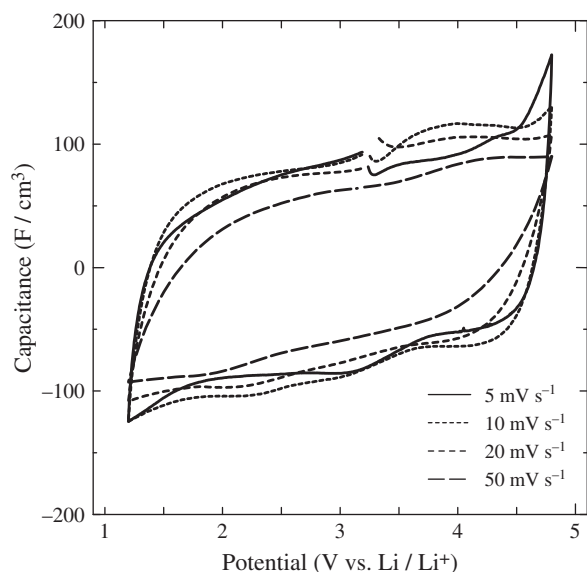
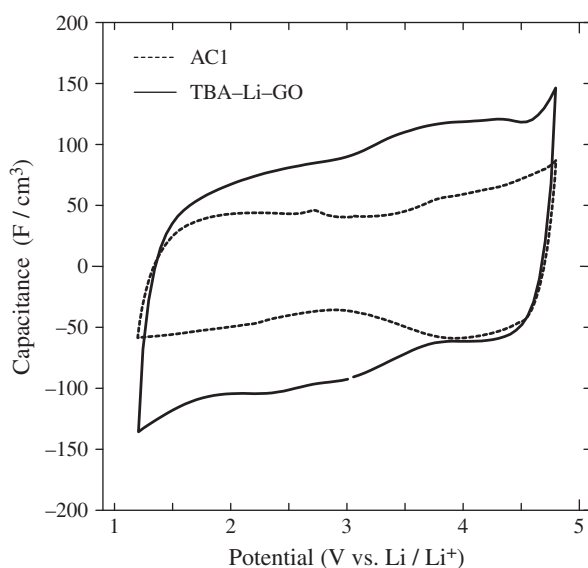**Fig. 13.** Cyclic voltammogram of TBA-Li-GO obtained in various scan rates.

Fig. 14. Cyclic voltammogram of TBA-Li-GO and AC1 obtained between potential range of 1.2–4.8 V within the scan rate of 10 mV s^{-1}.

showed very large internal resistance which is proved by the appearance of large semicircle. However, the internal resistance of the electrodes after cycles decreased dramatically. Especially for the electrode positive polarized at 4.8 V, the internal resistance became extremely low compared with that of other electrodes. As is stated above, the generation of new absorption sites for electrolyte ions after positive polarization might result in a low internal resistance.

However, different from polarized carbons, the TBA-Li-GO in our study still contains a certain amount of oxygen functional groups as it was proved by the FTIR results. Therefore, beside the generation of pores between the graphene layers, there is still the possibility that the residual oxygen containing groups in TBA-Li-GO could also contribute to the increased capacity after electrochemical activation. To see whether the decomposition of residual oxygen groups in TBA-Li-GO occurred or not upon cycling, the ex situ FTIR measurement of TBA-Li-GO electrode after cycling between OCV and 4.8 V was carried out and the results are shown in Fig. 12. It is can be seen from the FTIR profiles that the oxygen containing groups are still remaining in TBA-Li-GO electrode even cycled at high potential after 100 cycles. Aside from the difference in peak intensity, the peak position of TBA-Li-GO electrode after cycling is the same as that of pristine TBA-Li-GO. Moreover, it has been demonstrated that the contribution to the specific capacitance of oxygen containing groups can be neglected in organic electrolyte [44]. Therefore, we could exclude the possibility that the capacitance contribution result from the residual oxygen groups in TBA-Li-GO.

Fig. 13 presents the CV profiles of TBA-Li-GO with various scan rates in the range of 1.2–4.8 V. The CV curves of TBA-Li-GO are close to a rectangular shape at various scan rates, which is indicative of the typical double layer capacitor behavior. Moreover, there is no obvious capacitance loss even at the scan rate of 50 mV s^{-1}, which reveals the good rate capability of TBA-Li-GO electrode.

Fig. 14 displays the CV curves of TBA-Li-GO and AC1 electrode after 100 cycles. The CV curves of TBA-Li-GO keeps the rectangular shape as that of commercial AC1 even after 1000 cycles, which illustrates that the capacitor behavior is retained for TBA-Li-GO electrode. The capacitance of AC1 and TBA-Li-GO after 1000 cycles calculated from galvanostatic charge and discharge test and those from three electrodes are summarized in Table 2. Even though the extremely small surface area of TBA-Li-GO compared to that of AC1, TBA-Li-GO delivers high volumetric capacitance, 60 F cm^{-3} and 85 F cm^{-3} calculated from two electrode cell and three electrode cell, respectively. The volumetric capacitance of a single TBA-Li-GO after positive polarization at the first charge is almost two times than that of commercial AC1. The volumetric capacitance was calculated by only considering the density of the active material. As it was pointed out some other researchers that the expansion of the electrode after the electrochemical activation [45,46]. It is obvious that the electrochemical activation to cause a massive expansion of the electrode which would reduce the density of the active material. Further study is undergoing to investigate the dimensional change of TBA-Li-GO electrode after electrochemical activation by employing in situ dilatometry measurement.

electrolyte ions. In order to verify this assumption, the impedance spectra of TBA-Li-GO electrode cycled between OCV and 4.3 V, 4.5 V and 4.8 V after 100 cycles are present in Fig. 11. For comparison, the spectrum of electrode before cycling is also presented. The spectra of four different state electrodes show a semicircle at high frequency followed by the transition to linearity at low frequency region. The first semicircle implies the charge transfer resistance and the vertical line nearly 90° indicates purely capacitive behavior. By comparing the spectra it is obvious that the fresh electrode

Table 2
Physical properties and volumetric capacitance of AC1 and TBA-Li-GO.

Electrode material	BET surface area (m^2 g^{-1})	Tap density (g cm^{-3})	Specific capacity in two electrode cell (F cm^{-3})	Specific capacity in three electrode cell (F cm^{-3})
AC1	1400	0.38	36	45
TBA-Li-GO	16	0.85	60	85

4. Conclusions

We have synthesized spherical graphite oxide with MCMB as starting material. The morphology of the as-prepared GO kept the spherical shape even after mild oxidation. We are also able to determine the diameter of the pores generated in GO for the first time. It was found that thermal stability of neutralized GOs is improved extremely because of disappearance of heat evolution around 200 °C. Furthermore, the as obtained non-porous TBA-Li-GO shows an ideal EDLC feature and delivers high volumetric capacitance of 60 F cm^{-3} and 85 F cm^{-3} in two electrode cell and three electrode cell, respectively. The high capacitance of non-porous TBA-Li-GO may mainly be attributed to the generation of pores that are easily accessible to electrolyte ions after positive polarization at the first cycle. Moreover, the TBA-Li-GO obtained in this study does not require any kind chemical activation at high temperature such as that of activated carbons. Consequently, our study presents a feasible and low cost way for the synthesis of dense electrode materials.

References

[1] R. Kotz, M. Carlen, Electrochim. Acta 45 (2000) 2483–2498.
[2] P. Simon, Y. Gogotsi, Nat. Mater. 7 (2008) 845–854.
[3] E. Frackowiak, F. Beguin, Carbon 39 (2001) 937–950.
[4] A.F. Burke, John R. Miller, Electrochem. Soc. Interface 9 (2008) 53–57.
[5] V. Ruiz, C. Blanco, E. Raymundo-Pinero, V. Khomenko, F. Beguin, R. Santamaria, Electrochim. Acta 52 (2007) 4969–4973.
[6] S. Ishimoto, Y. Asakawa, M. Shinya, K. Naoi, J. Electrochem. Soc. 156 (2009) A563–A571.
[7] D. Qu, H. Shi, J. Power Sources 74 (1998) 99–107.
[8] S. Shiraishi, H. Kurihara, A. Oya, Carbon Sci. 1 (2001) 133–137.
[9] S. Shiraishi, H. Kurihara, L. Shi, T. Nakayama, A. Oya, J. Electrochem. Soc. 149 (2002) A855–A861.
[10] B. Fang, Y.Z. Wei, K. Maruyama, M. Kumagai, J. Appl. Electrochem. 35 (2005) 229–233.
[11] C. Lin, J.A. Ritter, B.N. Popov, J. Electrochem. Soc. 146 (1999) 3639–3643.
[12] C. Liu, A.J. Bard, F. Wudl, I. Weitz, J.R. Heath, Electrochem. Solid-State Lett. 2 (1999) 577–578.
[13] E. Frackowiak, K. Jurewicz, S. Delpeux, F. Beguin, J. Power Sources 97 (98) (2001) 822–825.
[14] S. Nomoto, H. Nakata, K. Yoshioka, A. Yoshida, H. Yoneda, J. Power Sources 97 (2001) 807–811.
[15] P. Simon, A. Burke, Electrochem. Soc. Interface (2008) 38–43.
[16] M.H. Liang, B. Luo, L.J. Zhi, Application of graphene and graphene-based materials in clean energy-related devices, Int. J. Energy Res. 33 (2009) 1161–1170.
[17] S. Stankovich, D.A. Dikin, G.H.B. Dommett, K.M. Kohlhaas, E.J. Zimmey, E.A. Stach, et al., Nature 442 (2006) 282–286.
[18] M.D. Stoller, S.J. Park, Y.W. Zhu, J.H. An, R.S. Ruoff, Nano Lett. 8 (2008) 3498–3502.
[19] Y.W. Zhu, S. Murali, W. Cai, X.S. Li, J.W. Suk, J.R. Potts, R.S. Ruoff, Adv. Mater. 22 (2010) 3906–3924.
[20] C. Liu, Z. Yu, D. Neff, A. Zhamu, B.Z. Jang, Nano Lett. 10 (2010) 3868–4863.
[21] M.M. Hantel, T. Kaspar, R. Nesper, A. Wokaun, R. Kotz, Electrochem. Commun. 13 (2011) 90–92.
[22] Y. Yamada, T. Imamura, H. Kakiyama, H. Honda, S. Oi, K. Fukuda, Carbon 12 (1974) 307–319.
[23] C. Zheng, J.C. Gao, M. Yoshio, L. Qi, H.Y. Wang, J. Power Sources 231 (2013).
[24] W.S. Hummers, R.E. Offeman, J. Am. Chem. Soc. 80 (1958) 1339.
[25] J.W. Lang, X.B. Yan, X.Y. Yuan, J. Yang, Q.J. Xue, J. Power Sources 196 (2011) 10472–10478.
[26] O.C. Compton, S.T. Nguyen, Small 6 (2010) 711–723.
[27] T. Nakajima, Y. Matsuo, Carbon 32 (1994) 469–475.
[28] Y. Matsuo, T. Miyabe, T. Fukutsuka, Y. Sugie, Carbon 45 (2007) 1005–1012.
[29] C. Hontoria-Lucas, A.J. Lopez-Peinado, J. de D. Lopez-Gonzalez, M.L. Rojas-Cervantes, R.M. Martin-Aranda, Carbon 33 (1995) 1585–1592.
[30] A. Lerf, H. He, T. Riedl, M. Forster, J. Klinowski, Solid State Ionics 101–103 (1997) 857–862.
[31] Y. Matsuo, Y. Nishino, T. Fukutsuka, Y. Sugie, Carbon 45 (2007) 1384–1390.
[32] Z.H. Liu, Z.M. Wang, X. Yang, K. Ooi, Langmuir 18 (2002) 4926–4932.
[33] T. Szabo, E. Tombacz, E. Illes, I. Dekany, Carbon 44 (2006) 537–545.
[34] M. Mermoux, Y. Chabre, A. Rousseau, Carbon 29 (1991) 469–474.
[35] A. Lerf, H. He, M. Forster, J. Klinowski, J. Phys. Chem. B 102 (1998) 4477–4482.
[36] M. Mermoux, Y. Chabre, Synth. Met. 34 (1989) 157–162.
[37] H.P. Boehm, Carbon 40 (2002) 145–149.
[38] Y. Matsuo, T. Miyabe, T. Fukutsuka, Y. Sugie, Carbon 45 (2007) 1005–1012.
[39] I.J. Kim, S.H. Yang, M.J. Jeon, S.I. Moon, H.S. Kim, Y.P. Lee, et al., J. Power Sources 173 (2007) 621–625.
[40] M. Takeuchi, K. Koike, T. Maruyama, A. Mogami, M. Okamura, Electrochemistry 66 (1998) 1311–1317.
[41] M. Takeuchi, T. Maruyama, K. Koike, A. Mogami, T. Oyama, H. Kobayashi, Electrochemistry 69 (2001) 487–492.
[42] B.H. Ka, S.M. Oh, J. Electrochem. Soc. 155 (2008) A685–A692.
[43] M.M. Hantel, T. Kaspar, R. Nesper, A. Wokaun, R. Kotz, Chem. Euro. J. 18 (2012) 9125–9136.
[44] T.A. Centeno, M. Hahn, J.A. Fernandez, R. Kotz, F. Stoeckli, Electrochem. Commun. 9 (2007) 1242–1246.
[45] H.D. Yoo, Y. Park, J.H. Ryu, S.M. Oh, et al., Electrochim. Acta 56 (2011) 9931–9936.
[46] M.M. Hantel, T. Kaspar, R. Nesper, A. Wokaun, R. Kotz, Electrochem. Commun. 34 (2013) 189–191.